The final, published version of the article can be accessed at http://dx.doi.org/10.1016/j.jhazmat.2020.123026

MOLECULARLY IMPRINTED FILMS AND QUATERNARY AMMONIUM-FUNCTIONALIZED MICROPARTICLES WORKING IN TANDEM AGAINST PATHOGENIC BACTERIA IN WASTEWATERS

Ana-Mihaela Gavrila[a#], Anamaria Zaharia[a#], Lisa Paruch[b], Francois Xavier Perrin[c], Andrei Sarbu[a], Andreea Gabriela Olaru[d***], Adam Mariusz Paruch[b**], Tanta-Verona Iordache[a*]

[a] *National Institute for Research & Development in Chemistry and Petrochemistry ICECHIM, Advanced Polymer Materials and Polymer Recycling Group, Splaiul Independentei 202, 060021, Bucharest, Romania*

[b] *Norwegian Institute of Bioeconomy Research (NIBIO), Division of Environment and Natural Resources, Fredrik A. Dahls vei 20, 1433 Aas, Norway*

[c] *Université de Toulon, Laboratoire Matériaux Polymères Interfaces et Environnement Marin-MAPIEM EA 4323 SeaTech-Ecole d'ingénieurs, BP 20132, 83957, La Garde Cedex, France*

[d] *S.C. EDAS-EXIM S.R.L., Banatului Street 23, 010933, Bucuresti, Romania*

[#]**These authors equally contributed to this work**

[*]**Correspondence to:** Advanced Polymer Materials and Polymer Recycling Group, The National Institute for R&D in Chemistry and Petrochemistry ICECHIM, PhD. Eng. Tanta-Verona Iordache, E-mail: Tanta-Verona.Iordache@icechim.ro

[**]**Correspondence to:** Norwegian Institute of Bioeconomy Research (NIBIO), Division of Environment and Natural Resources, Professor Adam Mariusz Paruch, E-mail: Adam.Paruch@nibio.no

[***]**Correspondence to:** S.C. EDAS-EXIM S.R.L., PhD biochem. Andreea Olaru, E-mail: Andreea.Olaru@edas.ro

ABSTRACT

Despite major efforts to combat pollution, the presence of pathogenic bacteria is still detected in surface water, soil and even crops due to poor purification of domestic and industrial wastewaters. Therefore, we have designed molecularly imprinted polymer films and quaternary ammonium-functionalized- kaolin microparticles to target specifically Gram-negative bacteria (GNB) and Gram-positive bacteria (GPB) in wastewaters and ensure a higher purification rate by working in tandem. According to the bacteriological indicators, a reduction by 90% was registered for GNB (total *coliforms* and *Escherichia coli* O157) and by 77% for GPB (*Clostridium perfringens*) in wastewaters. The reduction rates were confirmed when using pathogen genetic markers to quantify particular types of GNB and GPB, like *Salmonella typhimurium (reduction up to 100%),Campylobacter jejuni (reduction up to 70%) , Enterococcus faecalis (reduction up to 81%), Clostridium perfringens (reduction up to 97%)* and Shiga toxin-producing *Escherichia coli (reduction up to 64%)*. In order to understand the bactericidal activity of prepared films and microparticles, we have performed several key analyses such as Cryo-TEM, to highlight the auto-assembly mechanism of components during the films formation, and $^{29}Si/^{13}C$ CP/MAS NMR, to reveal the way quaternary ammonium grafted on the surface of kaolin microparticles.

Keywords: molecularly imprinted polymer films, quaternary ammonium-functionalized-kaolin microparticles, tandem bactericidal effect, wastewaters influent, pathogen genetic markers

1. INTRODUCTION

One of the current global problems relates to water quality and hazards for humans and the environment due to exposure to pathogenic bacteria from wastewaters. This issue has become very worrying because most pathogens responsible for critical waterborne diseases originate from faecal contamination due to inadequately treated or untreated domestic and industrial wastewater (Paruch et al., 2017**).** Furthermore, treated wastewater has been recently implemented in some European countries (Kalavrouziotis et al., 2011) as main source for crop irrigation and pathogenic bacteria can now be found

47 in soil and even crops (Ganoulis, 2012). Therefore, the fecal-oral transmission is the major route resulting
48 in contaminated food and polluted water through the transfer chain: feces-water/ soil/ environment-food-
49 humans.

50 Unfortunately, pathological agents are readily susceptible to resistance to classical antimicrobial
51 agents with small molecular masses used so far for wastewater purification. In addition, following
52 bactericidal diffusion, these small molecular biocides/disinfectants cause toxicity to the human organism
53 (Thomassin et al., 2007). Alternatively, antimicrobial polymeric materials provide a solution that
54 addresses these problems with both superior antimicrobial efficacy and reduced toxicity (Dong et
55 al., 2014, Xue et al., 2015). Moreover, chemical stability, non-volatility and long-term activity (Majumdar
56 et al., 2009) make polymers perfect candidates for implementing sustainable and environmentally friendly
57 solutions (Zheng et al., 2014) for wastewater decontamination. Of these, antimicrobial polymeric
58 materials containing quaternary ammonium salts (QAS) are some of the most effective and studied
59 antimicrobial polymers; over the last decade, there has been visible progress on development and
60 registration (Kenawy et al., 2007). It has also been demonstrated that polymers containing covalently
61 linked QAS have excellent and lasting bactericidal efficacy without contaminating the waters with
62 reactive fragments (Kumar et al., 2018). However, such materials have been more effective for the
63 inactivation of Gram-positive bacteria (GPB).

64 GPB contain a peptidoglycan-based layer composed of lipoteic acids that facilitate the penetration
65 of antimicrobial QAS moieties and subsequent membrane interaction, while Gram-negative bacteria
66 (GNB) have a cell wall composed of a single peptidoglycan layer surrounded by an outer membrane. This
67 latter membrane contains a toxic component called lipopolysaccharide (LPS) that acts as a barrier against
68 QAS-based biocides (Uday et al., 2014). Consequently, GNB shows higher resistance to QAS-based
69 biocides than GPB (Thoma et al., 2014). Thereby, other types of interfaces should be used to inactivate
70 GNB. For instance, molecular imprinting (Ye and Mosbach, 2008) has proved to be an intelligent
71 technique for designing synthetic antibodies, known as molecularly imprinted polymers (MIPs), that
72 generate specific recognition properties in a polymer matrix. The MIPs are endowed with specific

complementary cavities of the same shape and size but with complementary electronic entourage with a template molecule (or target molecule). These imprinted cavities allow only similar structures to be specifically retained in the polymer, from which, they can be later on removed by heating or washing with solvent without altering the geometry of the polymer (conferring reusability to the employed material). In this regard, methods like surface polymerization on magnetic particles (Jiang et al., 2016), thermo-nanoimprinted biomimetic probes (Buchegger et al., 2014) and MIP gels (Ogiso et al., 2013) have been used for specific proteins recognition.

With regard to the state-of-the-art on bactericidal materials, we report the original synthesis of molecularly imprinted polymer (MIP) films and quaternary ammonium-functionalized-kaolin microparticles (QAS-K MP) designed to work in tandem for the retention and inactivation of GNB and GPB pathogenic bacteria in wastewaters. In order to create QAS-K MP with bactericidal effect for GPB, we grafted the QAS groups on the surface of commercial kaolin microparticles by a two-step procedure; this assumed chemical modification of kaolin surface with vinyl groups, followed by free-radical polymerization of a QAS-containing monomer to create short QAS grafts. For the retention and inactivation of GNB, we proposed the use of MIP films with recognition cavities for lipopolysaccharides (LPS, the endotoxin component of GNB outer membrane). We prepared the MIP films *via* sol-gel derived methods using a functional organosilane as monomer and LPS from *Pseudomonas Aeruginosa* as template. The prepared materials were analysed morphologically, structurally and even thermally, using state-of-the-art methods, which helped explain the enhanced bactericidal efficiency in wastewaters (domestic and industrial).

2. EXPERIMENTAL DETAILS

2.1. Materials and methods

2.1.1. Materials for the bactericidal films and microparticles preparation

For films preparation, the functional organosilanic monomers [3- (2-trimethoxysilyl) - propylmethacrylate (MAPTES, 98%, Sigma Aldrich) and (3- Mercaptopropyl) trimethoxysilane (MPTES, 98%, Sigma Aldrich)], ammonium hydroxide - catalyst (NH4OH, 25 %, ChimReactiv), Ethanol (EtOH, 99.6%, Fisher Scientific), hydrochloric acid (HCl, 99.6%, Fisher Scientific) and distilled water were used as such. The lipopolysaccharide template from *Pseudomonas Aeruginosa 10* (LPS with 500,000 endotoxin units/mg, Sigma-Aldrich) was used in the form of lyophilized powder (as received).

For microparticles prepration, kaolin (K, ACROS Organics), vinyltrimethoxysilane (VTMS, 99%, Fluka), vinylbenzyl trimethylammonium chloride (VBTAC, 98%, Sigma Aldrich), 2,2′-Azobis (2-methylpropionitrile) (AIBN, 98%, Sigma Aldrich) radical initiator, ethanol (EtOH, 99.6%, Fisher Scientific), isopropanol (S.C. Reagents COM S.R.L) and dimethylforamide (DMF, 99.8%, Sigma-Aldrich) were used as such without any further purification.

2.1.2. Materials for genetic markers development

All developed genetic markers were achieved by standard cloning procedures using genomic DNA of the reference strains obtained from LGC Standards GmbH (Wesel, Germany). Pfx DNA polymerase (Invitrogen, California, USA) of high fidelity was used to amplify the target region of each marker. Zero Blunt® TOPO® PCR Cloning Kits (Invitrogen, California, USA) was used for cloning purpose. All the genetically transformed clones were validated and confirmed by DNA sequencing at Eurofins Genomics Germany GmbH (Ebersberg, Germany). The markers carrying plasmids were enriched and isolated using QIAprep Spin Miniprep Kit (Qiagen, Hilden, Germany). All applied primers and TaqMan probes were synthesized at Thermo Fisher Scientific (MA, USA), and their sequences are provided as supplementary information (S1). SsoAdvanced™ Universal Probes Supermix was used for the standard qPCR setup (Bio-Rad Laboratorie, Califonia, USA).

2.1.3. Materials for chemical and biochemical assays

Hach cuvette tests (Hach, Germany) were used for performing chemical analyses of WW samples, as follows: Chemical Oxygen Demand (COD) – LCI 400 (0-1000 mg/l Chemical Oxygen

Demand); LCK 339 Nitrate (0.23 - 13.50 mg/L NO3-N or 1 – 60 mg/L NO3); LCK 341 Nitrite (0.015 - 0.6 mg/L NO2-N or 0.05-2.0 mg/L NO2); LCK 303 Ammonium (2.0- 47 mg/L NH4-N or 2.5-60.0 mg/L NH4); LCK 350 Phosphorus total (2.0 - 20.0 mg/L PO4-P, 6.0 - 60.0 mg/L PO4 or 4.5 - 45.0 mg/L P2O5); LCK 338 LATON (20 - 100 mg/L Total Nitrogen, TNb). For the microbiological analysis, filter funnels with 47 mm filtration diameter, PES membranes (PALL filters 516-0427), Chrom Agar O157 (for identification of E coli O157), Chromatic E. Coli /Coliform Agar (for identification of total coliforms), and TSC agar plates (for differentiation of C perfringens) were purchased from Sanimed International.

2.2. Synthesis of lipopolysaccharide- molecularly imprinted polymer (LPS-MIP) films for GNB retention

In order to obtain layer-by-layer nano-assembled MIP films with LPS, the polymeric layers (one acting as interface and one as biomimetic film) were obtained in two steps by spraying directly on glass supports the precursor solutions, one at a time, according to a similar procedure described by Stoica et al. (Stoica et al., 2015). The usual recipe for films deposition by sol-gel technique involves the homogenization of two solutions at room temperature (25 °C), one containing the catalyst, meaning 25% ammonium hydroxide and distilled water (1.15 ml NH_4OH/ 0.45 mL H_2O) and, the other, the precursor organosilane monomers in ethanol. For the interface layer, MPTES (0.3 mL) was used as precursor monomer and ethanol (2 mL) as solvent. The precursor monomer solution was added gradually in the catalytic medium, at room temperature, under mechanical stirring at 200 rpm. After homogenization (t_{sg}= 2 h), the film precursor solution was sprayed directly onto degreased glass slides and left to rest 30 minutes at room temperature for the polycondensation to start. Subsequently, the LPS-MIP layer was sprayed on the interface layer following the same procedure used for the interface layer. In contrast, the LPS-MIP precursor solution contained MAPTES (0.2 mL meaning 0.64 mmoles) as monomer and 250,000 EU of LPS (as aqueous solution of 0.5 mg LPS/ 0.5 mL H_2O) as template for molecular imprinting, homogenised in 2 mL ethanol (a hazy solution was obtained due to monomer-LPS auto-assembly). The LPS-MIP film precursor solution was sprayed onto the previously coated glass slides and left for polycondensation to take place for 48 h at 25 °C, followed by maturation of films for 48 h at 55 °C

in an oven. In parallel, non-imprinted control films (noted by analogy NIPs) were synthesized respecting the same recipe but without adding LPS in the second step. All the films were washed with water (3 x 10 mL) for 4 hours using ultrasound; during this step LPS was also extracted from the MIP films, leaving behind cleaved affinity sites for the subsequent GNB retention and inactivation.

2.3. Synthesis of QAS-functionalized kaolin microparticles (K-VTMS-VBTAC) for GPB inactivation

QAS-functionalized kaolin microparticles (noted K-VTMS-VBTAC) were obtained in two steps. In the first step, the silylation reaction of Zaharia et al. (Zaharia et al., 2015) was adapted to obtain kaolin microparticles modified with vinyl-trimethoxysilane. In this respect, 1 g of kaolin microparticles (K) and 5 mL of vinyl-trimethoxysilane (VTMS) were introduced into a three-neck flask under nitrogen atmosphere. The reaction mixture was heated to 90, 150 or 190 °C under magnetic stirring (200 rpm). After 48 h, the mixture was cooled and the reaction product (K-VTMS) was recovered by centrifugation at 6000 rpm and washed with toluene (3 x 10 mL) in order to remove the excess silane. The product was dried in an oven at 105 °C until constant weight. Subsequently, QAS groups were tethered on the surface of the modified kaolin microparticles. For this step, vinylbenzyl-trimethylammonium chloride (VBTAC) as QAS groups generator was grafted *in situ* using AIBN as radical initiator of vinyl groups. For this matter, in a three-necked flask at reflux, 0.33 g of K-VTMS was introduced under N_2 atmosphere at 70 °C. A solution mixture consisting of 0.03 g of AIBN previously dissolved in 2 ml of EtOH/ DMF solvent mixture (50/50, vol.%) was added drop wise into the reaction flask. The temperature was kept constant at 70 °C for one hour under N_2 atmosphere, in order to generate free radicals on the surface of K-VTMS, after which, a solution consisting of 0.6 g VBTAC dissolved previously in 2 ml of EtOH/ DMF solvent mixture (50/50, vol.%) was added drop wise, as well, into the reaction flask. The reaction mixture was left at 70 °C under N_2 atmosphere. After 24 h, the reaction mixture was cooled down and the product (K-VTMS-VBTAC) was recovered by centrifugation at 6000 rpm and purified by washing with EtOH / DMF mixture (2 x 10 mL), in order to remove the unreacted monomer or non-grafted oligomers of VBTAC. Finally, the product was dried in an oven at 50 °C for 24 hours.

2.4. Employed characterisation methods for the bactericidal films and microparticles

The prepared bactericidal materials were first characterized morphologically, structurally and thermally using various instruments and methods.

Qualitative structural-compositional analysis of the prepared materials was performed using Fourier Transform Infrared Spectrometry (FTIR)- Bruker Tensor 37 (ATR) in the range 400-4000 cm^{-1} with a resolution of 4 cm^{-1} and a number of 16 scans. The spectra of materials were studied in KBr pellets.

The films precursor solutions were analayzed by Tecnai™ G2 F20 TWIN Cryo-TEM instrument (acceleration voltage of 120 kV, after confirming that the morphology is not affected by the large exposure). The procedure for Cryo-TEM investigation consisted of placing the sample (meaning aqueous solution of LSP and aqueous solution of LSP in contact with the functional monomer) on a carbon-film covered grid.

The morphological analysis was performed for the LPS-MIP and NIPs films using environmental scanning electron microscope (SEM, FEI Quanta 200 Instrument from Philips) equipped with a secondary electron detector in gaseous environment (GSED) and atomic force microscope (AFM, for Quantitative Mechanical Property Mapping at Nanoscale - PeakForce QNM) equipped with a silicon cantilever and an analyzer tip (having a nominal radius of 5 nm and a constant of elasticity of 5 N/ m). Ambient conditions: 1 Hz scan speeds and 90° scan angle. The LPS-MIP and NIP samples were dried for 3 h under vacuum at 40 °C prior morphological analysis.

Thermo-gravimetric analysis (TGA/ DTG) used for investigating the organic content grafted on the microparticles were performed on TA Instruments Q500 equipment, in the nitrogen atmosphere with a heating speed of 10 °C min^{-1}, in the 30-700 °C temperature range.

X-ray diffractograms (XRD) for the modified microparticles were obtained on Rigaku Diffractometer (Japan) using CuKa radiation with k = 0.1541 nm wavelength, for angles between 5 and 90 degrees.

196 Solid state ^{13}C CP/MAS NMR and ^{29}Si CP/MAS spectra were obtained on a Bruker Avance 400
197 MHz instrument. Approximately 100 mg of sample was packed into a 4 mm o.d. zirconia rotor. For ^{13}C
198 CP/MAS NMR experiments, the sample was spun at magic angle at 12 kHz and 1024 data points were
199 recorded over a spectral width of 300 ppm (ranging from-50 to250 ppm) with a 2.6 μs initial proton pulse
200 width and a 2 s relaxation delay; between 20000-40000 transients were acquired. ^{13}C chemical shifts were
201 referenced externally to TMS at 0 ppm by setting the downfield resonance of adamantane to 38.48 ppm.
202 For the ^{29}Si CP/MAS experiments, the sample was spun at the magic angle at 4 kHz. A simple block
203 decay experiment was employed with a 3 μs ^{29}Si pulse (90°) and a 58 kHz CW proton decoupling field
204 during the 50 ms acquisition time. The spectral width was fixed at 29762 Hz and CP contact time was 20
205 ms. Spectra were acquired with 34560 scans and 5 s recycle delay. The data collection time was 48 h.

206 *2.5. Markers development for GNB and GPB and their applications in pathogen screening*

207 To facilitate the detection of pathogenic bacteria more rapidly and accurately, real-time
208 quantitative polymerase chain reaction (RT-qPCR) have been employed for determination and
209 quantification of the pathogens by using genetic markers. In details, four pathogen markers have been
210 developed to target two GNB, i.e. *STM4497* for *Salmonella typhimurium* (*S. typhimurium*), *hipO* for
211 *Campylobacter jejuni* (*C. jejuni*); and two GPB, i.e. *16S rRNA* for *Enterococcus faecalis* (*E. faecalis*) and
212 *plc* for *Clostridium perfringens* (*C. perfringens*). In order to achieve a highly robust RT-qPCR assay in
213 practice, two pairs of primer sets were designed for each marker gene per pathogen in attempt to generate
214 two PCR amplicons at different sizes/lengths. In addition to these four aforementioned pathogen markers,
215 *stx1*, *stx2* and *eae* were developed for detection of Shiga toxin-producing *Escherichia coli* (STEC). The
216 details of respective genetic markers with the relevant references together with sequences of primers and
217 probes are presented in the results section. The final verified gene carrying plasmid was used as the
218 standards in downstream qPCR assays using derived serial dilutions. All generated qPCR amplification
219 efficiencies were between 90 – 100% with regression rate approaching 0,99. The raw qPCR data was

processed and analysed using CFX Manager Software built in CFX Connect™ Real-Time PCR Detection System (Bio-Rad Laboratories, Hercules, California, USA).

The applications of genetic markers were conducted in three-step trial. Firstly, 100 mL of both untreated and treated wastewater were concentrated by ultrafiltration to obtain the solid substances on the membrane filters (0,45 µm). Secondly, the resulted filters as whole (residues and filters) were used to extract microbial genomic DNA using DNeasy PowerWater kit (Qiagen GmbH, Hilden, Germany). The concentration of yielded DNA was measured on NanoDrop spectrophotometer (Ibekwe et al., 2002). In the third step, the developed markers were applied to detect the pathogens of GNB and GPB. The assay panel consisted of *S. typhimurium*, *C. jejuni*, *E. faecalis*, *C. perfringens* and *STEC*. qPCR was conducted in 20 µL reaction containing 10 µL SsoAdvanced™ Universal Probes Supermix (Bio-Rad Laboratories, Hercules, CA, USA), 500 nM of each primer, 250 nM 5'-FAM probe. The amplification conditions were as follows: 95 °C for 3 min, followed by 40 cycles of 95 °C for 15 s and 60 °C for 30 s.

2.6. Chemical and bacteriological testing methods

2.6.1. Wastewater sampling

Wastewater (WW) samples (noted SW and ALE) have been collected from the influent of two wastewater treatment stations (homogenization basin) and transported to the laboratory in the same day, in proper shipment conditions (controlled temperature and humidity). However, the research study on the efficiency of the two prepared bactericidal materials was further assessed using WW samples from the SW water plant (90% industrial water and 10% domestic sewage) as they contained both GNB and GPB (according to the pathogen screening in the ALE and SW water samples-Section 3.3.1). All the samples were used without pretreatment (no-disinfection or preliminary filtration) and analyzed within 2 h after collection.

2.6.2. Sample preparation for chemical and bacteriological analyses

The WW samples were analyzed before and after direct contact with the microparticles, films or both materials in tandem. Some of the microparticles and films were tested previously in order to establish the optimum method for evaluating the bactericidal efficiency. The targeted parameters were the contact time (within a 5-day study) and the WW sample volume (50 mL or 100 mL). After these preliminary tests, a total period of 24 h contact time was considered optimum for all the experiments and the volume of WW for testing the microparticles and films was different, meaning 100 mL of WW corresponding to 0.5 g of microparticles and 50 mL of WW corresponding to 1 film slide (with the total active surface of 12.5 cm^2). All the trials were performed in static isothermal conditions and the samples were analysed in triplicate. In the first step, microparticles and films were evaluated separately for their efficiency in WW. In a typical trial, 0.5 g microparticles (or 1 film slide) were placed into a cleaned glass vessel over which 100 mL (or 50 mL, respectively) of WW was poured. The vessel was sealed and left to rest in light-protected environment at room temperature (24 °C). After a period of 24 hours, the WW supernatant from the sample was collected, after sedimentation of microparticles, in a clean vessel and filtered using conventional membrane filtration methods (the film was extracted with tweezers from the vessel and the WW was filtered using membrane filtration methods). In order to evaluate the efficiency of the two materials in tandem we followed a similar procedure to that described for single treatment, with the difference that only 100 mL WW was contacted at room temperature (24 °C) with 0.5 g of microparticles and 1 film silde, in the following combination, treatment/tandem format (TF): K-VTMS-VBTAC + LPS-MIP (TF 1), K-VTMS-VBTAC + NIP (TF 2), MIP + K (TF 3) and NIP + K (TF 4). After a period of 24 hours, the film was extracted with tweezers from the vessel and the WW supernatant from the sample was collected, after sedimentation of microparticles, in a clean vessel and filtered using conventional membrane filtration methods. For filtering the WW samples, PES-membrane filters (PALL 516-0427, Φ 47 mm, pore size 0.45 μm) and a Labbox filtration system were used. The filtered WW was used for determining the chemical indicators and the PES-membrane filters for bacteriological indicators; the values were compared with those obtained for WW alone (as control sample).

2.6.3. Methods for chemicaland bacteriological analyses

Chemical analyses were performed for determining the key indicators of WW, before and after contact with the two materials in single and tandem formats, using commercial kits that employ standardized methods. In this respect, the measurement of COD concentration was performed by standardized photometric cuvette test from Hach (LCI 400), the total nitrogen (TN) content was determined by Hach cuvette test LCK 338 and the total phosphorus (TP) content by LCK 350. The total inorganic nitrogen (TIN) was calculated as sum of all inorganic forms of nitrogen, as follows: the nitrogen from ammonia determined by Hach LCK 303, the nitrogen from nitrates by Hach LCK 339 and the nitrogen from nitrites by Hach LCK 341. The procedures for determining each parameter were respected according to the indications provided in the kit and are detailed in **Text S1 Chemical Indicators**. Whenever specified in the cuvette kits instructions, digestion of samples was performed with a Hach Thermostat LT200. For direct concentrations measurements, a Spectrophotometer Hach Lange DR 3800 (wavelength 190-1100 nm) was used.

For performing the bacteriological analyses, the PES-membrane filters were placed on agar plates to be ensured that no air bubbles were trapped between the membrane filter and the medium. Filter disks were transferred to the chromogenic/TSC agar plates and incubated at 44 °C± 0.5 °C for 24 h (Hach Incubator). The results were red within 15 minutes after removing the disks from the incubator. The colonies were counted using a colony counter (Funke Gerber). More details about the methods are given in **Text S2 Bacteriological indicators**.

3. RESULTS AND DISCUSSION

3.1. Lipopolysaccharide-molecularly imprinted polymer (LPS-MIP) films for GNB retention

3.1.1. Synthesis of bactericidal LPS-MIP films

The organosilica interface and the LPS-MIP film were obtained in two steps using sol-gel derived techniques (**Fig. 1**). The sol-gel method is one of the most promising and versatile techniques in materials

292 science because it allows designing materials with unique properties at low temperatures. Generally, the
293 sol-gel technique is a process involving the transition from a liquid "sol" (a colloidal particle suspension)
294 to a solid system called "gel". In our study, layer-by-layer polymeric films were applied by spraying the
295 obtained precursor solutions directly on commercial glass slides. In the first step, an interface layer was
296 prepared followed by tethering the LPS-MIP layer; both layers cured by polycondensation reactions
297 according to **Fig. 1**a and c. The proposed imprinting mechanism with LPS for the preparation of LPS-
298 MIP films is depicted in **Fig. 1**b. LPS is a short peptide composing the endotoxin membrane of GNB that
299 contains at top the *O*-antigen, which can act as active group in the molecularly imprinting “epitope”
300 approach. The *O*-antigen is the primary structural constituent of lipopolysaccharides (King et al., 2014),
301 being a repeating oligosaccharide unit with *β*-D-galactose, *β*-D-galactosamine and *β*- glucosamine
302 groups. While the MPTES monomer was chosen for its ability to acts as a primer (Pape, 2011**)** between
303 the glass slides and the actual LPS-MIP film, the MAPTES monomer was chosen for the content of
304 methacryloxy functional groups that are more prone to interact with the hydroxyl and amine groups from
305 the *O*-antigen of LPS. According to Apicella et al. (Apicella et al., 1994), LPS can form micelles of 10-20
306 kDa in the presence of strong surface-active agents and absence of divalent cations, due to the self
307 aggregation function of lipid A component of the LPS molecule. This behavior was also observed in our
308 study (micrographs in **Fig. 2)** where LPS assembled with the MAPTES monomer. Considering these
309 observations, the most probable molecular imprinting mechanism was based on non-covalent interactions
310 between the monomer and the *O*-antigen (as presented in **Fig. 1**b). Following the LPS-MIP curing, the
311 extraction of LPS (**Fig. 1**d) was performed in order to generate active sites for GNB inactivation.

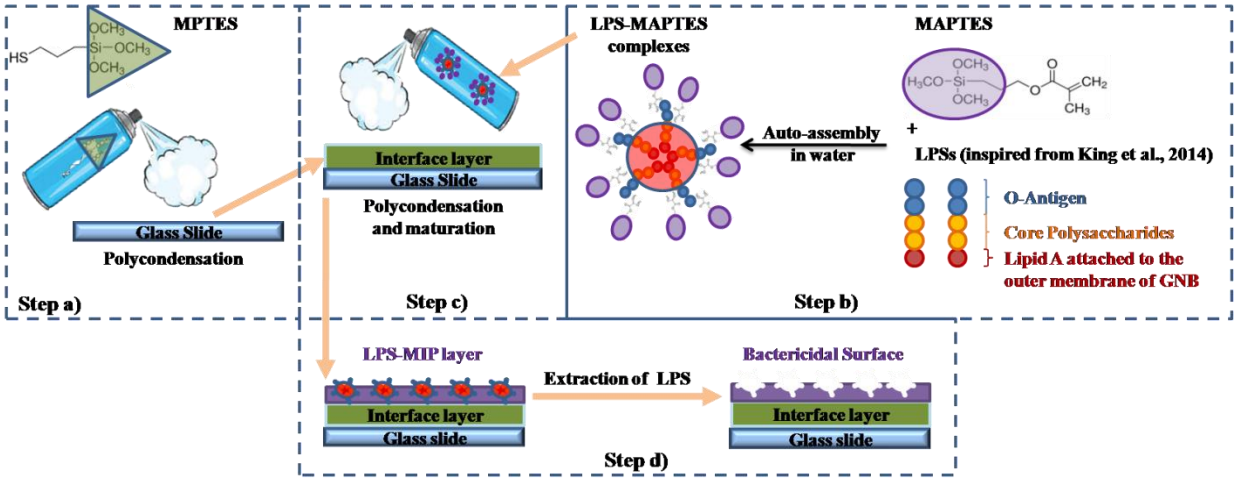

312

313 **Fig. 1.** Preparation of layer-by-layer assembled films by polycondensation: Step a) procedure for casting
314 the interface layer, Step b) MAPTES and LPS auto-assembly in the precursor solution for MIP films with
315 the formation of non-covalent polymerizable complexes, Step c) procedure for casting and curing of LPS-
316 MIP, and Step d) Extraction of LPS with the formation of active sites.

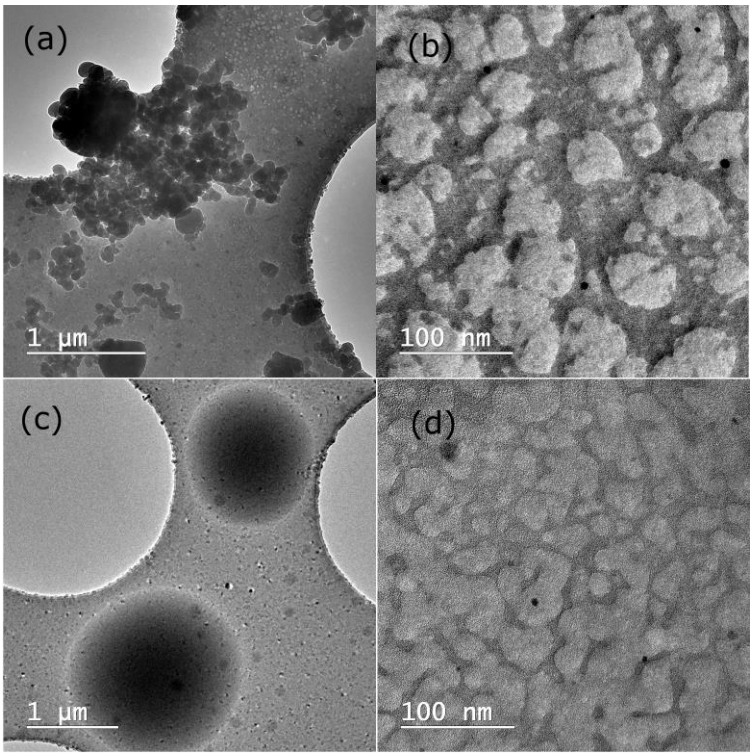

317

Fig. 2. Cryo-TEM images at different magnitudes of (a, b) LPS in water [0.5 mg LPS/ 0.5 mL H_2O, as used in the original recipe] and of (c, d) LPS in water after MAPTES monomer addition [0.2 mL as used in the original recipe]

3.1.2. Structure of bactericidal LPS-MIP films

FTIR spectroscopy was used to highlight changes in the structure of the new materials after the physical or chemical modifications. Using this method, the efficiency of the washing procedures was also followed, for NIP and LPS-MIP. Hence, the LPS-MIP, MIP Ex and the corresponding non-imprinted NIP homologue were structurally analysed and compared with the spectrum of the LPS template molecule (**Fig. S1,** where MIP-Ex is the notation of LPS-MIP after the extraction of LPS template molecules).

Comparing the FTIR spectra of all polymeric films, some similarities were observed. Due to the fact that the films differ only by the presence of the template, the basic composition of the polymers does not undergo major changes. The stretching vibrations characteristic to the main polymer backbone, $\nu_{\text{-CH2}}$ and $\nu_{\text{-CH-}}$, recorded in the 2922-2935 cm^{-1} and 670-695 cm^{-1} region were observed in the spectrum of both LPS-MIP, before and after LPS extraction, and that of NIP film. The characteristic bands of the $(SiO)_n$ backbone were recorded in the 1240-850 cm^{-1} wavenumber region (bands overlapping in the spectra of LPS-MIP, MIP-Ex and NIP polymers). Several bands of the polymers and those of LPS overlap, i.e. C=O, C-O, -CH and even –OH (Parikh and Chorover, 2007). Yet, the presence of LPS in the MIP film was indicated by the stretching vibrations characteristic to N-H bonds ($\nu_{\text{-NH-}}$, from the two glucosamine groups) and to P=O recorded at 3409 cm^{-1} (wide band) and 1254 cm^{-1} (sharp band), respectively, in the spectrum of LPS-MIP; these two bands disappear/flatten after template extraction (spectrum of MIP Ex).

3.1.3. Morphology of bactericidal LPS-MIP films

The morphological analysis of films on glass slides considered the use of two specific techniques, i.e. scanning electron microscopy (SEM, **Fig. 3** and **Fig. S2**) and atomic force microscopy (AFM, **Fig. S3** and **Fig. S4**). Considerable differences were observed between the LPS-MIP films and the control NIP films, which pointed-out to the monomer-template auto-assembly prior polycondensation. The MAPTES-

LPS complex led to the formation of flower-shaped structures on the LPS-MIP surface (**Fig. 3**a), validating the hypothesis of micelles formation. Together with the FTIR and TEM, these results proved that LPS presence in the precursor film solution impacted the growth mechanism of sol-gel matrix and, thus, the MIP films architecture. Nevertheless, it is important to note that all the films, particularly the LPS-MIP films, showed very good adhesion and compatibility with the glass substrate. In addition, it was observed that all the films were continuous with no fractures (**Fig. S2)**.

The AFM analysis (**Fig. S3** and **Fig. S4)** also provided proof towards the homogeneity (Wei et al., 1998) of LPS-MIP films. It can be observed that the surface of the LPS-MIP film (**Fig. S3**a) presented discrete porous arrangements. Thus, the LPS-MIP composition led to an interesting nanometric structural architecture (**Fig. S4**) compared to the more flattened and non-homogenous morphology of the NIP (**Fig. S3**b and **Fig. S4**). At the same time, the specific porosity can be better observed on the topography of LPS-MIP films (**Fig. S3**c), where pores of 200 nm in diameter and 4.5 nm in depth can be distinguished. The topography of films after scratching (**Fig. S4**) revealed the thickness of films i.e. 2.5 µm and 2.6 µm respectively for MIP and NIP, which was in agreement to the estimated one (Stoica et al., 2019). As a result, AFM analysis corroborated with SEM demonstrated that LPS influences the formation mechanism of the sol-gel matrix and also favours the appearance of specific porous structures.

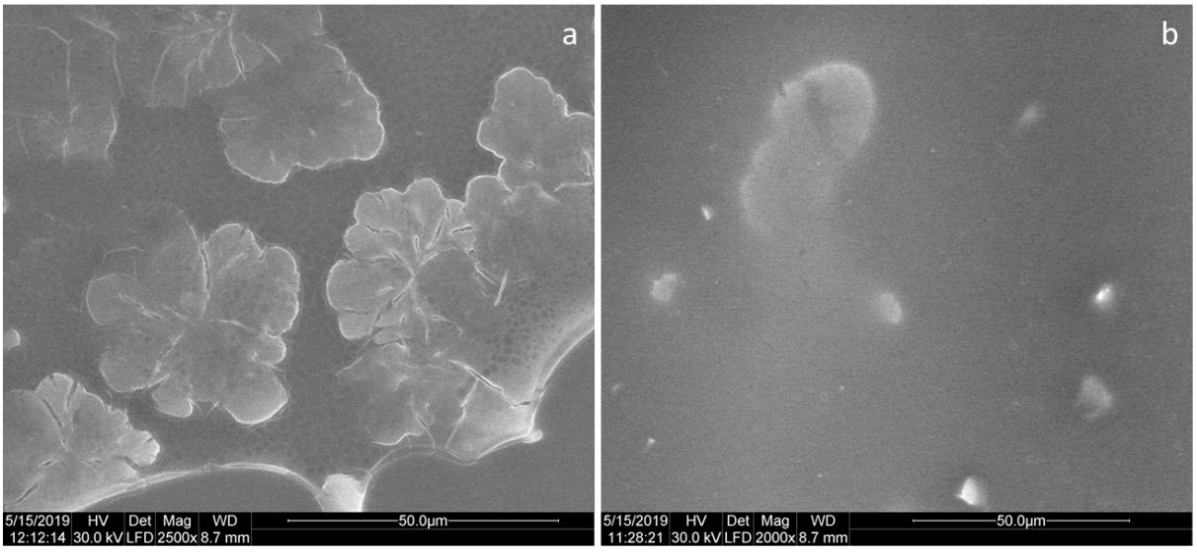

Fig. 3. SEM images of films deposited on glass slides a) LPS-MIP film; b) NIP film;

3.2. QAS-functionalized kaolin microparticles for GPB inactivation

3.2.1. Synthesis of QAS-functionalized kaolin microparticles

The silylation reaction with VTMS was performed in order to insert chemically a significant amount of vinyl groups on the surface of kaolin to serve as grafting nods for the following functionalization with QAS –based monomers. The process was performed in two steps according to **Fig. 4**. In the first step silylation was performed similarly to the recipe described by Zaharia et al. (2015), but using VTMS as functional silane, bearing both vinyl groups (the grafting nods for QAS) and methoxy groups (which interact chemically with the hydroxyl surface groups of kaolin in the silylation reaction). The second step assumed the existence of vinyl groups on the surface of kaolin, which were activated with AIBN, and served as grafting points for the radical addition/polymerization of VBTAC; this functional monomer is bearing both vinyl groups (involved in the radical grafting) and QAS groups (which serve as bactericidal functionalities for GPB).

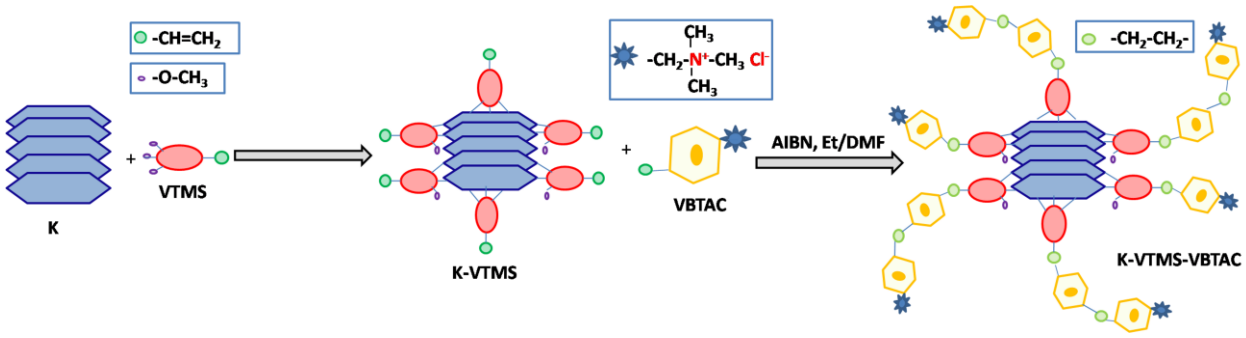

Fig. 4. Preparation of QAS-modified kaolin particles by silylation with vinyltrimethoxysilane and radical grafting of vinylbenzyltriamonium monomers

3.2.2. Structure of QAS-functionalized kaolin microparticles

During the preparation of microparticles, the structure modification after each step, i.e. (i) surface modification of kaolin by silylation with VTMS and (ii) grafting of VBTAC, was analyzed.

The characteristic FTIR spectra of kaolin alone (K) and modified kaolin with VTMS (K-VTMS) at different reaction temperatures (90, 150, 190 °C) are shown in **Fig. S5**a. The spectra of all modified K-

VTMS samples showed characteristic bands of kaolin (at 3695, 3612 cm^{-1} and between 1250-500 cm^{-1} range) as well as bands from VTMS in the range of 2925 cm^{-1}- 2847 cm^{-1}, 1604 cm^{-1} and 1412 cm^{-1} characteristic for the stretching vibrations of CH_2, C=C and C-O, respectively. It should be mentioned that for the K-VTMS sample functionalized at 190 °C additional structures were formed; the appearance of bands at 1729 and 1630 cm^{-1} characteristic for carbonyl groups, suggested that the increase of silylation temperature led to oxidation of grafted vinyl groups. Therefore, lower values for the temperature should be employed in order to graft VTMS on the surface of kaolin without affecting the vinyl functionalities. The spectrum of K-VTMS-VBTAC in **Fig. S5**b, presents the same characteristic bands of kaolin in the two formerly-mentioned regions, i.e. 3695-3612 cm^{-1} and 1250-750 cm^{-1}. Bands from VTMS, characteristic for -CH_2- stretching, appear between 2956 and 2844 cm^{-1}, and the ones for C=C (vinyl) at 1637 cm^{-1}. The presence of VBTAC is represented by the highly characteristic band from 1630 cm^{-1}, assigned to the stretching vibrations of the C=C bonds corresponding to the aromatic nucleus (Campos et al., 2014**)**. The grafting procedure was, hence, successful as the band corresponding to C=C (corresponding to vinyl groups from VTMS) disappeared and the band of C=C (corresponding to the aromatic nucleus of VBTAC) appeared instead.

Further on, the XRD spectra of kaolin samples modified with VTMS (K-VTMS) at different reaction temperatures (90, 150, 190 °C) were identical to those of K alone (**Fig. S6**). All three K-VTMS samples and K-VTES-VBTAC showed characteristic diffraction peaks for kaolin at 7.1 and 3.5 Å, according to the reported literature data (Castellano et al., 2010**)**. This result confirmed the fact that VTMS was grafted onto the surface of the kaolin without affecting the intralamellar space of K (as intercalation with small molecules may occur according to Zaharia et al., 2015).

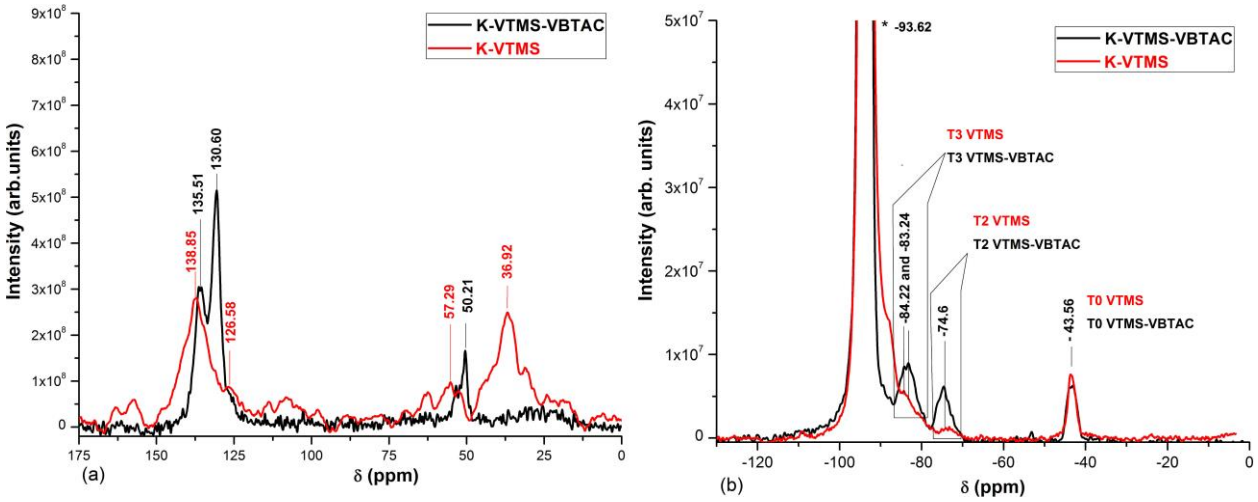

Fig. 5. (a) CP-MAS ^{13}C -NMR of kaoline after silylation with VTMS at 150 °C (K-VTMS red at 10 kHz) and after grafting the quaternary amonium salt (K-VTMS-VBTAC black at 12 kHz); (b) CP-MAS ^{29}Si spectra of kaoline after silylation with VTMS at 150 °C (K-VTMS red at 12 kHz) and after grafting the quaternary amonium salt (K-VTMS-VBTAC black at 12 kHz);

The CP MAS ^{13}C -NMR and ^{29}Si spectra of K-VTMS at 150 °C and of K-VTMS-VBTAC provided supplementary evidence for the chemical grafting of vinyl-trimethoxysilane to kaolin (*via* hydroxyl surface groups) followed by VBTAC radical addition to the vinyl double bond of VTMS (**Fig. S5**). In the CP MAS ^{13}C -NMR spectrum of K-VTMS (**Fig. S5**a) characteristic vinyl signals were observed at 126.58 and 138.85 ppm. The signal at 57.29 ppm detected in the spectrum of K-VTMS was due to rigidly fixed methoxy groups grafted onto the aluminol surface of kaolin (Al-OMe) and no signals assigned to hydrolyzed methoxy groups were detected at 49-50 ppm, thus confirming the successful silylation reaction at 150 °C. In **Fig. 5**a the amount of grafted VTMS was very low and, hence, different magnetic fields were applied for acquisition of spectra. Thereby, the intensity of signals from CH, CH_2 and CH_3 groups was lower in the spectrum of K-VTMS-VBTAC. In the CP-MAS ^{29}Si spectra at 12 kHz of K-VTMS and K-VTMS-VBTAC (**Fig. 5**b) the signal at -93.62 ppm is attributed to Q units of O-Si-O from kaolinite as suggested by Elbok and Detellier (Elbok and Detellier, 2009). The ^{29}Si peak of the VTMS T° structure was also shifted to -43.56 ppm from -60 ppm (the non-grafted VTMS) which suggests

a chemical modification of VTMS according to Jain *et* al. (Jain et al., 2005). The CP MAS ^{29}Si spectrum of K-VTMS (**Fig. 5**b) also validated the chemical grafting of VTMS *via* T2 (74.6 ppm) and T3 (84.22 and 82.24 ppm) grafts; the T2 type of grafts explaining the presence of methoxy groups (36.92 ppm) in **Fig. 5**a. It is also interesting to notice that no signal was detected for T1 grafts (around -65 ppm) (Jain et al., 2005).

Farmore, after VBTAC addition (**Fig. 5**a**)** the vinyl signals of VTMS were replaced by the specific signals of carbon from the aromatic double bond at 135.51 and 130.60 ppm and by the signal from C-$N^{+}(CH)_3$ group in VBTAC at 50.21 ppm (Espiritu et al., 2017). No signals from VBTAC monomer, at 140.1 ppm and 116 ppm due to CH= and CH2= groups, respectively, were recorded (Zajac et al., 2019), which suggested that the registered signals of carbon belong only to grafted VBTAC. In addition, the increase of intensity on T2 and T3 grafts registered on CP MAS ^{29}Si spectrum of K-VTMS-VBTAC also suggested that VBTAC was grafted on the initial VTMS vinyl grafts (**Fig. 5**b).

3.2.3. Thermogravimetric analysis of QAS-functionalized kaolin microparticles

Thermogravimetry was an additional method used to underline the modification of K with VTMS and the subsequent grafting of VBTAC. Furthermore, using the values of mass loss registered after each modification step the number of QAS units on a single graft could be approximated. In this respect, K alone, K-VTMS (sample prepared at 150 °C) and K-VTMS-VBTAC were analysed and TGA/ DTG curves were plotted according to **Fig. S7**b and c.

Kaolin presented only one major stage of thermal degradation that was attributed to the kaolin dehydroxylation process (transformation into meta-kaolinite), with a maximum temperature of 510 ºC (Avila et al., 2010). For K-VTMS microparticles, two thermal degradation stages were observed. The first stage of thermal degradation, in the range of 375-390 ºC, was associated with the decomposition of grafted VTMS on the kaolin surface and the second step, between 450-660 ºC, corresponded to dehydroxylation of kaolin (**Fig. S7**b). In accordance with FTIR, K-VTMS at 90 ºC contained lower amounts of grafted VTMS compared to the K-VTMS at 150 ºC, and K-VTMS at 190 C presented the

highest organic content as a result to the former statement regarding oxidation of VTMS vinyl groups. Therefore, the following experiments with VBTAC modification were carried-out using only the optimum recipe of K-VTMS at 150 ºC.

The DTG characteristic diagram for K-VTMS-VBTAC decomposition (in **Fig. S7**c) presented two stages of thermal degradation, as well. The first occurred in a range of 352-390 °C, which corresponded to the decomposition process of grafted VBTAC and fragments of VTMS (e.g. -O-Si-CH_2-CH_2-) and the second decomposition was characteristic for kaolin dehydroxylation. It is also important to mention that the mass loss increased in the series: K < K-VTMS < K-VTMS-VBTAC.

Considering the mass loss of K, K-VTMS (at 150 °C) and K-VTMS-VBTAC, meaning 10.7 wt.%, 11.6 wt.% and 13.7 wt.%, the quantity of grafted VTMS and VBTAC at 100 g of product (K-VTMS or K-VTMS-VBTAC) may be approximated. Therefore, in 100 g of K-VTMS product, 0.7 g represents the grafted VTMS (difference of mass loss between K-VTMS and K alone) meaning 6 mmoles of VTMS [the molecular mass, *M,* of 116 g/mole for double point grafted VTMS having the formula H_3C_2-Si-$O_2(OCH_3)$ was considered for this determination]. Following the same mechanism and considering the difference of mass loss between K-VTMS and K-VTMS-VBTAC, results 2.1 g VBTAC in 100g of K-VTMS-VBTAC product, meaning 10.6 mmoles of grafted VBTAC [having the formula H3C2(C6H4)N(C3H9)Cl, *M*=197 g/mol]. Looking at the two resulted values, it is striking to notice that the molar ration of VTMS: VBTAC is approximately 1:1.8 indicating two probable scenarios for the grafting. The most obvious one implies the formation of dimmers instead of having a single molecule of VBTAC grafted on VTMS and the second one takes into account that only some of the vinyl groups of VTMS were initiated and the following grafting step led to the formation of VBTAC oligomers (which were washed-out during the purification procedure). Since, the latter is not sustained by CP-MAS ^{13}C RMN (no vinyl signals of VTMS present), the results indicated towards grafting of VBTAC in the form of dimmers. This would explain the enhanced bactericidal effect of microparticles (highlighted in Section 3.3). Hence, these findings provided important information regarding the achievement of surface modification with VTMS and the subsequent grafting with VBTAC.

3.3 Evaluation of films and microparticles bactericidal efficiency

3.3.1. Pathogen screening in the ALE and SW water samples

Initial pathogen screening assays indicated that the overall pathogen load in SW was relatively larger than in ALE, as reflected by harbouring one order magnitude higher of *E. faecalis* (1,59E+04 copies/100 mL vs. 7,20E+03 copies/100 mL) and two orders higher of *S. typhimurium* (5,69E+06 copies/100 mL vs. 4,91E+04 copies/ 100mL). However, ALE had higher numbers of *C. perfringens* (7,17E+03 copies/100 mL) in comparison to SW (2,97E+02 copies/100 mL). *C. jejuni* was detected in neither of the wastewater. Based on this preliminary screening, the SW wastewater source was selected for the subsequent chemical and bacteriological tests.

3.3.2. Chemical and bacteriological evaluation of wastewater supernatants

In the first step, each sample of WW taken from the SW source was contacted with either LPS-MIP and NIP films or with the K-VTMS-VBTAC and control-K microparticles. **Table 1** summarizes the results obtained for the chemical and bacteriological tests conducted according to the methods described in the Experimental part- Section 2.6.

The elimination of pathogenic bacteria from the WW constitutes an advanced treatment process that is usually carried out using “disinfection” processes, which assumes the penetration of the disinfectant, through the cell wall and attacking the key proteins from the protoplasm. This “disinfection” process is here highlighted by the increase of total nitrogen and Kjeldahl nitrogen, while the decrease of the TP content is more likely linked to the adsorption capacity of the materials to bind phosphates present in the SW. Therefore, after 24 h of contact with the LPS-MIP film, the chemical indicators, meaning COD and TP were lower with approximately 20% and 60%, respectively and the bacteriological indicators of WW decreased with approximately 63% for *coliforms*, 100% for *E coli* O157 and 74% for *C. perfringens*, compared to the values determined for the control WW sample (SW). For the NIP films, the chemical and bacteriological indicators of WW also decreased but in lower extents (except for TP and *E coli* O157) compared to the LPS-MIP. In this respect, the COD and TP decreased with approximately

17% and 65%, respectively and the *coliforms*, *E coli* O157 and *C. perfringens* were reduced by 50%, 100% and 60% respectively. Further on, the same chemical and bacteriological indicators were found to decrease for the K-VTMS-VBTAC and K materials, as well. The COD and TP chemical indicators were lower with approximately 15% and 42%, respectively for K-VTMS-VBTAC and with approximately 22% and 47%, respectively for K, while the bacteriological indicators for *coliforms*, *E coli* O157 and *C. perfringens* were reduced by 82%, 67% and 65%, respectively, for K-VTMS-VBTAC and by approximately 71%, 100% and 30%, respectively, for K. Hence, based on this preliminary biochemical evaluation of microparticles and films, it can be stated that LPS-MIP films are quite efficient for both GNB and GPB retention. As for the microparticles, the results show that K-VTMS-VBTAC is indeed more efficient for GPB bacteria inactivation compared to K alone.

Table 1

Chemical and bacteriological indicators evaluated for LPS-MIP/NIP films and K-VTMS-VBTAC/control-K microparticles after 24 h contact with SW sourced WW, and the standard error of means (SE) for each trial set

Indicator	**WW source SW[1,2]**	**LPS-MIP[2]**	**NIP[2]**	**K-VTMS-VBTAC[2]**	**K[2]**
Chemical oxygen consumption (COD±SE), mg L^{-1}	**11275.0**±17.21	**9104.7**±272.68	**9320.0**±337.22	**9549.0**±201.50	**8751.7**±202.28
Ammoniacal nitrogen (NH4-N±SE), mg L^{-1} Nitrogen	14.60±0.02	14.79±0.06	14.92±0.13	27.47±0.38	22.43±0.43
from Nitrates (NO3-N±SE), mg L^{-1}	3.24±0.01	3.45±0.06	2.53±0.9	3.37±0.04	3.28±0.07
Nitrogen from Nitrites (NO2-N±SE), mg L^{-1}	1.56±0.01	1.71±0.07	1.59±0.02	1.17±0.06	1.12±0.04
Total nitrogen ($N_{inorganic}$±SE), mg L^{-1}	19.40±0.04	19.95±0.13	19.04±0.11	32.01±0.41	26.83±0.52
Kjeldahl nitrogen	239.20±0.18	287.17±9.86	279.21±2.12	267.46±4.53	261.27±20.92

(KN±SE), mg L^{-1}					
Total nitrogen (TN±SE), mg L^{-1}	244.00±0.20	292.33±9.82	283.33±2.19	272.00±4.58	265.67±21.67
Total phosphorus (TP±SE), mg L^{-1}	**57.70**±0.02	**23.12**±0.87	**20.10**±0.17	**33.90**±1.44	**31.20**±1.08
***E coli O157*±SE, CFU·100 mL^{-1}**	**1.00**±0.00	**0.00**±0.00	**0.00**±0.00	**0.33**±0.33	**0.00**±0.00
***Total Coliforms*±SE, CFU·100 mL^{-1}**	**120.00**±0.03	**45.00**±7.09	**60.33**±6.64	**26.33**±5.50	**34.67**±6.33
***C. perfringens*±SE, CFU·100 mL^{-1}**	**82.00**±0.02	**21.00**±1.52	**33.00**±4.36	**29.33**±3.48	**57.67**±3.18

[1] the volume of wastewater was 50 mL/ 1 film slide and 100 mL/0.5 mg of microparticles

[2]the measurements (M) were performed in triplicate and the standard error of means, SE (±) was calculated with the relation $SD/(n^{1/2})$, where n is the number of experiments (3), SD is the standard deviation $SD=(M\Delta(\Sigma_n{}^2)/(n-1))^{1/2}$, $M\Delta_n$ the deviation of data from the mean value.

The first results showed that the efficiency of LPS-MIP films developed initially for GNB retention/ inactivation were successful for GNB reduction up to 81.5% (63% coliforms and 100% *E.coli* retention) and also successful for GPB reduction up to 74% (74% *C. perfringens* retention), whilst the K-VTMS-VBTAC developed for GPB retention/ inactivation were successful for GNB reduction up to 73.5% (82% coliforms and 67% *E.coli* retention) and only 65% successful for GPB reduction (65% *C. perfringens* retention). Hence, it is notable that the molecularly imprinted materials have gain ground over the more known QAS-based materials, which proved to be very efficient for GPB, as well. However, when the two types of materials were combined into the TFs, a synergic bacteria-destruction mechanism was activated (see **Table 2**). The chemical indicators, meaning COD and TP were decreased with approximately 28% and 60%, respectively for the TF 1 (the one composed from LPS-MIP and K-VTMS-VBTAC) system and with approximately 23% and 60%, respectively for the TF 4 (the reference-composed from NIP and K), while the bacteriological indicators, meaning *coliforms*, *E coli* O157 and *C. perfringens* were reduced by 80%, 100% and 77% respectively for the TF 1 system and with approximately 33%, 100% and 54% respectively for the TF 4 system. Therefore, the synergic efficiency

528 of the TF 1 system developed for the tandem GNB and GPB retention/ inactivation was the most
529 successful for GNB and GPB reduction, with 90% and 77%, respectively.

530 **Table 2**

531 Chemical and bacteriological indicators evaluated for the following combination, treatment/tandem
532 format (TF): TF1 (LPS-MIP + K-VTMS-VBTAC) and TF2 (NIP + K-VTMS-VBTAC), and their
533 respective references with K alone, i.e.: TF3 (MIP + K) and TF4 (NIP + K), after 24 h contact with SW
534 sourced wastewater, and the standard error of means (SE) for each trial set

Indicator	**WW source SW[1,2]**	**TF1[2]**	**TF2[2]**	**TF3[2]**	**TF4[2]**
Chemical oxygen consumption (COD±SE), mg L^{-1}	**11275.0**±17.21	**8121.0**±170.36	8550.0±220.24	8244.0±217.39	8653.0±186.83
Ammoniacal nitrogen (NH4-N±SE), mg L^{-1}	14.60±0.02	19.23±0.03	20.69±0.06	21.55±0.12	22.75±0.18
Nitrogen from Nitrates (NO3-N±SE), mg L^{-1}	3.24±0.01	3.11±0.04	3.09±0.05	3.26±0.04	2.78±0.06
Nitrogen from Nitrites (NO2-N±SE), mg L^{-1}	1.56±0.01	1.78±0.02	1.52±0.04	1.32±0.01	1.39±0.03
Total nitrogen ($N_{inorganic}$±SE), mg L^{-1}	19.40±0.04	24.12±0.13	25.30±0.12	26.13±0.23	26.92±0.17
Kjeldahl nitrogen (KN±SE), mg L^{-1}	239.20±0.18	263.11±5.32	289.39±4.77	294.42±6.05	296.83±5.78
Total nitrogen (TN±SE), mg L^{-1}	244.00±0.20	268.00±5.21	294.00±4.09	299.00±6.14	301.00±5.98
Total phosphorus (TP±SE), mg L^{-1}	**57.70**±0.02	**23.40**±0.65	22.21±0.79	24.66±0.95	22.99±1.02
***E coli O157*±SE, CFU·100 mL^{-1}**	**1.00**±0.00	**0**±0.00	0±0.00	0±0.00	0±0.00
***Total Coliforms*±SE, CFU·100 mL^{-1}**	**120.00**±0.03	**24.0**±3.54	30.0±3.68	66.0±2.33	81.0±2.01
***C. perfringens*±SE, CFU·100 mL^{-1}**	**82.00**±0.02	**19.0**±1.65	27.0±2.35	45.0±2.08	36.0±1.81

535 [1] the volume of wastewater was 100 mL/ (1 film slide and 0.5 mg of microparticles)

[2]the measurements (M) were performed in triplicate and the standard error of means, SE (±) was calculated with the relation SD/($n^{1/2}$), where n is the number of experiments (3), SD is the standard deviation SD=($M\Delta(\Sigma_n{}^2)/(n-1))^{1/2}$, $M\Delta_n$ the deviation of data from the mean value.

3.3.3. Genetic marker-based pathogen detections and removal efficiency estimations on wastewater treated with different nanostructural strategies

The obtained raw data was processed and converted according to the dilution factor of each sample to copy numbers (CN) pr. 100ml as shown in **Table 3**. The individual pathogen removal rate (RR) presented in percentage was estimated as [(CN of untreated SW – CN of treated with respective material or TF)/CN of untreated SW]. The pathogen eliminating effectiveness was assessed towards GPB and GNB. With regard to GPB, the reduction of *E. faecalis* in wastewater treated by LPS-MIP and K-VTMS-VBTAC demonstrated higher efficiency than the other materials, with RR at 81% and 82% respectively (**Table 3**). As for *C. perfringens*, NIP and K-VTMS-VBTAC represented better performances with RR at 85% and 68% respectively. The lowest removal efficiency was determined in the treatment with kaolin alone (**Table 3**), which was in great relation with outcomes of the bacteriological tests also reporting the lowest reduction of *C. perfringens* (**Table 1**). Concerning GNB, 75% of *S. typhimurium* was removed in wastewater treated by K-VTMS-VBTAC as compared to 59% achieved by K alone (**Table 3**). Besides, LPS-MIP and NIP exhibited considerably high efficiency towards clearance of *S. typhimurium* with similar RR at 67% and 66% respectively. Since *C. jejuni* was not detected in raw SW, thus no further assays were performed on the treated samples. As for the removal of STEC, which was evaluated based on the quantification of three genetic markers, i.e. *stx1*, *stx2* and *eae*, the wastewater samples treated with K-VTMS-VBTAC and K resulted in lower amount of CN of these markers than those treated with LPS-MIP and NIP, RR ranging from 26% to 60%). Overall, LPS-MIP and K-VTMS-VBTAC presented higher efficacy in elimination of targeted GPB and GNB. Based on the results acquired from the initial individual testing on different materials (films and microparticles), further investigation was conducted to evaluate the "tandem effect" yielded from the TF combinations of films and microparticles (**Table 3**).

After contact with SW for 24 h, TF1 and TF2 could remove the GPB at high rates, i.e. *E. faecalis* at respectively 81% and 55% and *C. perfringens* at respectively 97% and 66%. The highest removal rate was achieved by TF1 and this corresponds greatly with the highest reduction revealed by the biological tests (**Table 2**).

Table 3

Genetic marker-based pathogens presented in copy numbers (CN) with the standard error of means (SE) for each trial set and their removal rate (RR) in percentage during treatment of wastewater by different materials and combinations of treatment/tandem format (TF)

Materials and treatment/ tandem formats	***Enterococcus faecalis*** **CN ± SE/ 100ml**	**RR**	***Clostridium perfringens*** **CN ± SE/ 100ml**	**RR**	***Salmonella typhimurium*** **CN ± SE/ 100ml**	**RR**	***Campylobacter jejuni*** **CN ± SE/ 100ml**	**RR**	**Shiga toxin-producing *Escherichia coli* (STEC) *stx1*** **CN ± SE/ 100ml**	**RR**	***stx2*** **CN ± SE/ 100ml**	**RR**	***eae*** **CN ± SE/ 100ml**	**RR**
SW[1]	2.31E+03 ± 4E-01	-	2.38E+02 ± 0E-02	-	1.40E+06 ± 4E+01	-	0.00E+00 ± 0E+00	-	3.57E+05 ± 3E+01	-	8.12E+04 ± 7E+00	-	2.85E+03 ± 1E-02	-
LPS-MIP	4.48E+02 ± 1E-01	81	1.48E+02 ± 6E-02	38	4.58E+05 ± 2E+00	67	0.00E+00 ± 0E+00	-	3.52E+05 ± 0E+01	1	8.63E+04 ± 0E+00	0	2.79E+03 ± 4E-01	2
NIP	7.18E+02 ± 4E-02	69	3.66E+01 ± 4E-02	85	4.72E+05 ± 5E+00	66	0.00E+00 ± 0E+00	-	3.56E+05 ± 1E+00	0	8.39E+04 ± 4E+00	0	1.21E+03 ± 8E-01	58
SW[2]	7.80E+03 ± 0E-02	-	4.95E+02 ± 9E-01	-	2.18E+07 ± 2E+02	-	0.00E+00 ± 0E+00	-	4.91E+05 ± 7E+01	-	9.75E+04 ± 3E+00	-	4.18E+03 ± 0E-01	-
K	3.47E+03 ± 7E-01	56	3.54E+02 ± 5E-01	29	9.06E+06 ± 5E+02	59	0.00E+00 ± 0E+00	-	2.86E+05 ± 5E+00	42	6.43E+04 ± 2E+00	34	1.66E+03 ± 1E-02	60
K-VTMS-VBTAC	1.37E+03 ± 1E-02	82	1.60E+02 ± 2E-02	68	5.51E+06 ± 7E+01	75	0.00E+00 ± 0E+00	-	3.01E+05 ± 5E+00	39	7.18E+04 ± 9E+00	26	2.09E+03 ± 3E-01	50
SW[3]	7.12E+03 ± 7E-01	-	9.73E+02 ± 6E-01	-	6.21E+05 ± 7E+01	-	1.02E+03 ± 5E-01	-	4.56E+06 ± 1E+01	-	2.87E+05 ± 4E+00	-	7.16E+03 ± 9E+00	-
TF1	1.34E+03 ± 4E-01	81	2.99E+02 ± 4E-01	97	0.00E+00 ± 0E+00	100	3.06E+02 ± 9E-02	70	1.40E+06 ± 4E+02	69	8.19E+04 ± 4E-01	71	3.40E+03 ± 0E-01	53
TF2	3.18E+03 ± 7E-01	55	3.33E+02 ± 1E-01	66	0.00E+00 ± 0E+00	100	1.48E+03 ± 8E-01	0	1.54E+06 ± 1E+01	66	6.73E+04 ± 4E+01	76	3.63E+03 ± 4E+00	49
TF3	1.25E+04 ± 5E+00	0	7.49E+02 ± 4E-04	23	1.34E+06 ± 6E+01	0	2.82E+03 ± 6E-01	0	2.31E+06 ± 5E+01	49	1.90E+05 ± 6E+00	34	5.96E+03 ± 0E-01	17
TF4	1.44E+04 ± 7E+00	0	2.89E+02 ± 2E-01	0	9.97E+05 ± 7E+00	0	1.00E+04 ± 1E-01	0	2.88E+06 ± 8E+01	37	2.03E+05 ± 9E+01	29	5.82E+03 ± 0E-01	18

[1] wastewater raw material used for film trial

[2] wastewater raw material used for microparticle trial

[3] wastewater raw material used for tandem trial (TF)

[4] the details of respective genetic markers with the relevant references together with sequences of primers and probes are presented in **Table S1**

With regard to the "tandem effect" on GNB removal, 100% elimination of *S. typhimurium* was achieved in both TF1 and TF2 (**Table 3**). Interestingly, TF1 could remove 70% of *C. jejuni*, but no efficiency was observed in TF2. Worth to note, that among all these aforementioned pathogens' analyses, all the references, i.e. TF3 and TF4 showed no any effect on reduction of any of these target pathogens in SW, except 23% reduction of *C. perfringens* in TF3 (**Table 3**). As for the STEC investigation, all types of treatment formats worked on reducing contents of *stx1*, *stx2* and *eae* markers, however, TF1 and TF2 functioned apparently superior to their respective references **(Table 3).**

Overall, these findings evidenced that the combined and optimized tandem application of LPS-MIP with K-VTMS-VBTAC (TF1) could substantially enhance the treatment capabilities and efficiency in mitigating pathogenic burden in wastewater, which constitute the serious public health threat. There are no published data on establishing and applying the LPS-MIP layers and QAS-modified kaolin for municipal wastewater treatment, thus the achieved results of pathogen removal are quite original and, hence, difficult to be compared/discussed with outcomes of other related studies. Yet some similarities can be observed with regard to pathogens inactivation in different nanomaterials applied to wastewater treatment. Copper nanoparticles were reported as extremely efficient in inhibiting and destroying both gram-positive/-negative microorganisms (Dlamini et al., 2019). Gram-negative bacterium *E. coli* was excellently removed from wastewater using mesoporous nanocomposite films (Seo et al., 2012), also single-walled carbon nanotubes demonstrate strong antibacterial activities resulting in *E. coli* bacterial cell death (Liu et al., 2009).

4. CONCLUSIONS

This paper describes an application of innovative materials for wastewater treatment with a particular focus on removal of pathogens represented by GNB and GPB. The materials synthesis constitutes the core novelty of the study with LPS-molecularly imprinted films and kaolin microparticles modified with QAS groups, both designed in an original way to inactivate GNB and GPB, respectively.

The bacteriological assessment indicated that the films prepared following the molecular imprinting technologies, using LPS to create the bactericidal effect, were highly performant against GNB with a reduction rate of 81.5% (63% coliforms and 100% *E.coli*) and also successful for GPB reduction up to 74% (*C. perfringens*). Nevertheless, the QAS-functionalized kaolin microparticles prepared by the two-step grafting procedure has emerged as a new way to create highly efficient materials for GPB inactivation, for which, the reduction rate was 65% (*C. perfringens*). While various removal efficiencies of pathogens were observed during application of single treatment formats, the combined formats (tandem) resulted in higher treatment efficiencies. The highest removal rates were revealed especially by tandem application of LPS-MIP with K-VTMS-VBTAC, by 80%, 100% and 77% for *coliforms*, *E coli* O157 and *C. perfringens*, respectively. Even the chemical indicators, meaning COD and TP were decreased with approximately 28% and 60%, respectively for this tandem format.

The overall efficiency of LPS-MIP and K-VTMS-VBTAC in elimination of targeted GPB and GNB was confirmed by specific analyses of pathogens using genetic markers. Hence, after contact with SW for 24 h, the tandem format could remove the GPB and GNB at high rates, i.e. *Enterococcus faecalis* at 81%, *Clostridium perfringens* at 97%, *Salmonella typhimurium* at 100%*, Campylobacter jejuni* at 70% and Shiga toxin-producing *Escherichia coli* at 69% (according to *stx1* marker), 71% (according to *stx2* marker) and 53% (according to *eae* marker).

The obtained results are unprecedented as there are no related studies on the synthesis and application of such type of hybrid materials for municipal wastewater treatment. Thus, these findings present novel insights into the synthesis methodologies of the two materials (LPS-MIP films and K-VTMS-VBTAC microparticles), treatment technologies, efficiency assessments and scientific approaches toward removal of GNB and GPB.

Funding: This work was supported by the M-ERA.NET network, the European Union and the National Authorities UEFISCDI (Romania, ctr. no. 71/2017) and RCN (Norway) [for funding the project TANDEM nr. 4155 under the M-ERA.NET2 co-funded Call 2016] and by UEFISCDI (Romania) [for funding the national ctr. no. TE123 / 2018–BACTERIOSENS].

Credit Author Statement

Authors' individual contributions, using the relevant CRediT roles, are: **Conceptualization-** Tanta Verona Iordache; **Formal analysis, Investigation-** Ana Mihaela Gavrila, Anamaria Zaharia, Francois Xavier Perrin and Lisa Paruch; **Methodology-** Tanta Verona Iordache, Ana Mihaela Gavrila, Anamaria Zaharia, Andreea Gabriela Olaru and Adam Mariusz Paruch; **Supervision, Project administration, Funding acquisition, Resources, Validation, Visualization, Writing - original draft, Writing - review & editing -** Tanta Verona Iordache, Adam Mariusz Paruch and Andreea Gabriela Olaru.

Declaration of competing interest

The authors declare that they have no known competing financial interests or personal relationships that could have appeared to influence the work reported in this paper.

Data statement

A part of the raw/processed data required to reproduce these findings cannot be shared at this time being part of an ongoing study. Some of the raw data can be found in the **Supplementary Material**.

References

Apicella M.A. Griffiss J.M., Schneider H., 1994. Isolation and characterization of lipopolysaccharides, lipooligosaccharides, and lipid A. Methods Enzymol. 235:242-52.

Avila, L.R., de Faria, E.H., Ciuffi, K.J., Nassar, E.J., Calefi, P.S., Vicente, M.A., Trujillano, R., 2010. New synthesis strategies for effective functionalization of kaolinite and saponite with silylating agents. J. Colloid Interf. Sci. 341 (1), 186-193.

Buchegger, P., Lieberzeit, P.A., Preininger, C., 2014. Thermo-nanoimprinted biomimetic probe for LPS and LTA immunosensing. Anal. Chem. 86, 1679-1686.

Campos, C.H., Urbano, B.F., Rivas, B.L., 2014. Hybrid composites from poly[(4-vinylbenzyl)trimethylammonium chloride]–metal oxide using simultaneous radical polymerization/sol–gel synthesis. Mater. Lett. 131, 198–202.

Castellano, M., Turturro, A., Riani, P., Montanari, T., Finocchio, E., Ramis, G., Busca, G., 2010. Bulk and surface properties of commercial kaolins. Appl. Clay Sci. 48 (3), 446-454.

Dlamini, N.G., Basson, A.K., Pullabhotla, V.S.R., 2019. Optimization and Application of Bioflocculant Passivated Copper Nanoparticles in the Wastewater Treatment. Int. J. Environ. Res. Public Health 16 (12), E2185.

Dong, C., Ye, Y., Qian, L., Zhao, G., He, B., Xiao, H., 2014. Antibacterial modification of cellulose fibers by grafting β-cyclodextrin and inclusion with ciprofloxacin. *Cellulose* 21,1921–1932.

Elbok, T., Detellier, C., 2009. Kaolinite-poly(methacrylamide) intercalated nanocomposite via in situ polymerization. Canadian J. Chem. 87, (1) 272-279.

Espiritu, R., Golding, B. T., Scott, K., Mamlouk, M., 2017. Degradation of Radiation Grafted Hydroxide Anion Exchange Membrane Immersed in Neutral pH: Removal of Vinylbenzyl Trimethylammonium Hydroxide due to Oxidation. J. Mater. Chem. A 5, 1248– 1267.

Ganoulis, J., 2012. Risk analysis of wastewater reuse in agriculture. *Int. J. Recycl. Org. Waste Agric.* 1, 3.

Ibekwe, A.M., Watt, P.M., Grieve, C.M., Sharma, V.K., Lyons S.R., 2002. Multiplex fluorogenic real-time PCR for detection and quantification of Escherichia coli O157:H7 in dairy wastewater wetlands. Appl. Environ. Microbiol. 68 (10), 4853-62.

665 Jain, S., Goosens, H., Picchioni, F., Magusin, P., Mezari, B., Van Duin, M., 2005. Synthetic aspects and
666 characterization of polypropylene-silica nanocomposites prepared via solid-state modification and
667 sol-gel reactions. Polymer 46, 6666–6681.
668 Jiang, H., Jiang, D., Shao. J., Sun, X., 2016. Magnetic molecularly imprinted polymer nanoparticles based
669 electrochemical sensor for the measurement of Gram-negative bacterial quorum signaling
670 molecules (N-acyl-homoserine-lactones). Biosens Bioelectron. 75, 411-419.
671 Kalavrouziotis, I.K., Arambatzis, C., Kalfountzos D., Varnavas S.P., 2011. Wastewater Reuse Planning in
672 Agriculture: The Case of Aitoloakarnania, Western Greece. Water 3, 988-1004.
673 Kenawy, E.R., Worley, S.D., Broughton, R., 2007. The chemistry and applications of antimicrobial
674 polymers: A state-of-the-art review. Biomacromolecules 8, 1359–1384
675 Kumar, A., Boyer, C., Nebhani, L., Wong, E.H.H., 2018. Highly Bactericidal Macroporous Antimicrobial
676 Polymeric Gel for Point-of-Use Water Disinfection. Sci. Rep. 8, 7965.
677 King, J.D., Berry, S., Clarke, B.R., Morris, R.J., Whitfielda, C., 2014. Lipopolysaccharide O antigen size
678 distribution is determined by a chain extension complex of variable stoichiometry in Escherichia
679 coli O9a, Proc Natl Acad Sci USA 111(17), 6407–6412.
680 Liu, S., Wei, L., Hao, L., Fang, N, Chang, M.W., Xu, R., Yang, Y., Chen, Y., 2009. Sharper and faster
681 “Nano darts” kill more bacteria: a study of antibacterial activity of individually dispersed pristine
682 single-walled carbon nanotube. ACS Nano 3(12), 3891–3902.
683 Majumdar, P., Lee, E., Gubbins, N., Stafslien, S.J., Daniels, J., Thorson, C.J., Chisholm, B.J., 2009.
684 Synthesis and antimicrobial activity of quaternary ammonium-functionalized POSS (Q-POSS) and
685 polysiloxane coatings containing Q-POSS. Polymer 50, 1124–1133.
686 Ogiso, M., Aiba, S.-I., Minoura, N., 2013. Preparation of Molecularly Imprinted Polymer Gel Beads for
687 Adsorption of Endotoxin, Kōbunshi Rombunshū 70 (2), 82-86.
688 Parikh, S.J., Chorover, J., 2007. Infrared spectroscopy studies of cation effects on lipopolysaccharides
689 in aqueous solution. Colloids Surf B Biointerfaces 55 (2) 241–250.

690 Paruch, L., Paruch, A.M., Blankenberg, A.G.B., Haarstad, K., Mæhlum, T. 2017. Norwegian study on
691 microbial source tracking for water quality control and pollution removal in constructed wetland
692 treating catchment run-off. Water Sci. Technol. 76(5), 1158-1166.
693 Pape, P.G., 2011. Plastics Design Library. In Ebnesajjad, S. (Ed.) Handbook of Adhesives and Surface
694 Preparation, Technology, Applications and Manufacturing, William Andrew Applied Science
695 Publishers, Cap 15 - Adhesion Promoters, Pages 369-386.
696 Seo, Y.I., Hong, K.H., Kim, S.H., Chang, D., Lee, K.H., Kim, Y.D., 2012. Removal of bacterial pathogen
697 from wastewater using Al filter with Ag-containing nanocomposite film by in situ dispersion
698 involving polyol process. J. Hazard Mater. 15 (227-228), 469-473.
699 Stoica, E.B., Gavrila, A.M., Branger, C., Brisset, H., Dyshlyuk, A.V., Vitrik, O.B., Iovu, H., Sarbu, A.,
700 Iordache, T.V., 2019. Evaluation of Molecularly Imprinted Thin Films for Ephedrine recognition,
701 Mater. Plast. 4: 865-874.
702 Thoma, L.M., Boles, B.R., Kuroda, K., 2014. Cationic methacrylate polymers as topical antimicrobial
703 agents against *Staphylococcus* aureus nasal colonization. Biomacromolecules 15, 2933–2943.
704 Thomassin, J.M., Lenoir, S., Riga, J., Jérôme, R., Detrembleur, C., 2007. Grafting of poly[2-(*tert*-
705 butylamino)ethyl methacrylate] onto polypropylene by reactive blending and antibacterial activity
706 of the copolymer. Biomacromolecules 8, 1171–1177.
707 Uday, S.P., Thiyagarajan, D., Goswami, S., Adhikari, M.D., Das, G., Ramesh, A., 2014. Amphiphile-
708 mediated enhanced antibiotic efficacy and development of a payload nanocarrier for effective
709 killing of pathogenic bacteria. J. Mater. Chem. B. 2, 5818–5827.
710 Wei, Y., Jin, D., Brennan, D. J., Rivera, D. N., Zhuang, Q., DiNardo, N. J., Qiu, K., 1998. Atomic Force
711 Microscopy Study of Organic-Inorganic Hybrid Materials. Chem. Mater. 10, 769-772.
712 Xue, Y., Xiao, H., Zhang, Y., 2015. Antimicrobial Polymeric Materials with Quaternary Ammonium and
713 Phosphonium Salts. Int. J. Mol. Sci. 16, 3626–3655.
714 Ye, L., Mosbach, K., 2008. Molecular Imprinting: Synthetic Materials as Substitutes for Biological
715 Antibodies and Receptors. Chem. Mater. 20 (3), 859-868.

716 Zaharia, A., Perrin, F.X., Teodorescu, M., Radu, A.L., Iordache, T.V., Florea, A.M., Donescu, D., Sarbu,
717 A., 2015. New organophilic kaolin clays based on single-point grafted 3-aminopropyl
718 dimethylethoxysilane. Phys.Chem.Chem.Phys. 17, 24908-24916.
719 Zajac, A., Szpechta, A., Zielinski, D., Rola, K., Hoppea, J., Komorowska, K., Smiglak, M., 2019.
720 Synthesis and characterization of potentially polymerizable amine-derived ionic liquids bearing 4-
721 vinylbenzyl group. J. Molec. Liq. 283, 427-439.
722 Zheng, A., Xue, Y., Wei, D., Li, S., Xiao, H., Guan, Y., 2014. Synthesis and characterization of
723 antimicrobial polyvinyl pyrrolidone hydrogel as wound dressing. Soft Mater. 12, 179–187.